Electronic Spectra of Cs_2NaYbF_6 and Crystal Field Analyses of YbX_6^{3-} (X = F, Cl, Br)

Xianju Zhou,[†] Michael F. Reid,[‡] Michèle D. Faucher,[§] and Peter A. Tanner*[,†]

Department of Biology and Chemistry, City University of Hong Kong, Tat Chee Avenue, Kowloon, Hong Kong S.A.R., PRC, and Department of Physics, University of Canterbury, Christchurch, New Zealand

Received: December 12, 2005; In Final Form: May 27, 2006

Detailed analysis of the vibronic structure in the electronic absorption spectrum of Cs_2NaYbF_6 at temperatures between 10 and 300 K enables the crystal field energy level diagram of Yb^{3+} in this cubic host to be deduced. Ultraviolet and visible laser excitation of Cs_2NaYbF_6, $Cs_2NaY_{0.9}Yb_{0.1}F_6$, and $Cs_2NaHo_{0.99}Yb_{0.01}F_6$ give spectral features mainly due to Yb^{3+} being situated at a range of defect sites. The $4f^{13}$ crystal field analyses of octahedral YbX_6^{3-} (X = F, Cl, Br) systems show the expected trends in parameter values, but the energy level fits are poor. Inclusion of the interaction with the charge-transfer configuration $4f^{14}np^5$ provides an exact fitting of energy levels for YbX_6^{3-}, and a smooth variation of ff and fp crystal field parameters for $Cs_2NaLnCl_6$ (Ln = Er, Tm, Yb) is observed.

Introduction

The elpasolites, M_2ALnX_6 (M, group I metal; A, group I metal; Ln, lanthanide ion; X, halogen) are model systems for the study of the optical spectra and energy levels of Ln^{3+}. This is because the Ln^{3+} ion is situated at a site of high symmetry (O_h molecular symmetry point group) which confers a high degree of degeneracy to the energy levels and introduces restrictive selection rules for the optical spectra. Whereas extensive experimental studies have been performed upon the hexachloroelpasolite systems, $Cs_2NaLnCl_6$,[1] there are few reports of the optical spectra of the corresponding hexafluoroelpasolite systems. The previous major works have studied the vibrational spectra of Cs_2KLnF_6,[2] the magnetic properties of M_2ALnF_6,[3,4] and luminescence and two photon absorption studies of Cs_2NaYF_6:Eu^{3+} [5,6] and Cs_2NaTbF_6.[6,7] The present study aims to extend these works by the investigation of the energy levels of Yb^{3+} in hexafluoroelpasolite lattices. It was of major interest to see if the simple system comprising one electron hole (where atomic Hamiltonian parameters are not present) could be well-modeled by standard $4f^N$ crystal field theory. It turns out that the inclusion of configuration interaction with a charge-transfer configuration is required to obtain a satisfactory data fit.

Experiment

Cs_2NaYbF_6, Cs_2NaYF_6:Yb^{3+} (10 atom %), Cs_2NaHoF_6:Yb^{3+} (1 atom %) were purchased from N. M. Khaidukov, who prepared them by hydrothermal synthesis.[5] Electronic absorption spectra were obtained at resolution 2 cm^{-1}, by a Biorad FTS-60A spectrometer, equipped with a Si detector. Emission spectra were recorded using a tunable pulsed laser (Panther OPO system pumped by the third harmonic of a Surelite Nd:YAG laser). The signal was collected at 90° by an Acton 0.5 m monochromator, with a grating blazed at 750 nm (600 groove/mm), and a back-illuminated SpectruMM CCD detector. All experiments were carried out between room temperature and 10 K, with the sample housed in an Oxford Instrument closed cycle cryostat.

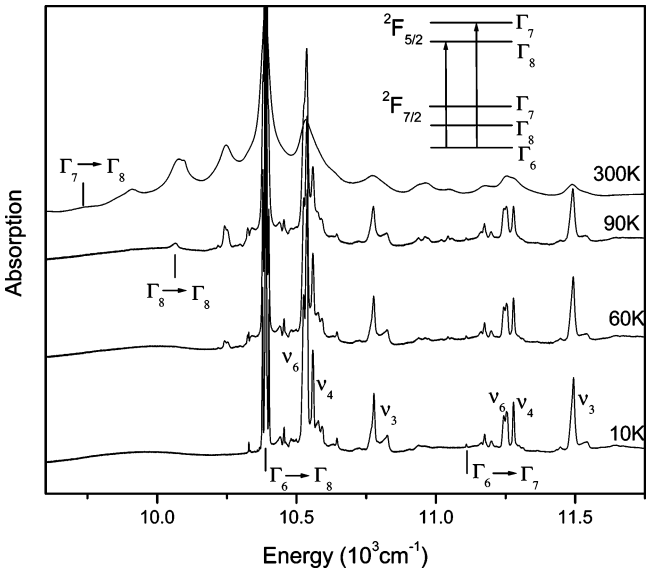

Figure 1. $^2F_{7/2} \rightarrow {}^2F_{5/2}$ electronic absorption spectrum of Cs_2NaYbF_6 at various temperatures between 10 and 300 K. The electronic origins and associated vibrational structure are marked.

Results and Discussion

Electronic Spectra. Figure 1 shows the electronic absorption spectrum of Cs_2NaYbF_6 at various temperatures between 10 and 300 K. It is assigned analogously to the spectrum of $Cs_2NaYbCl_6$.[8] The two electronic transitions which are observed at 10 K are depicted in the inset of the figure, and the electronic origins are marked on the spectrum. Note that the intense $^2F_{7/2}$ $\Gamma_6 \rightarrow \Gamma_8$ $^2F_{5/2}$ transition is magnetic-dipole allowed, whereas the very weak $^2F_{7/2}$ $\Gamma_6 \rightarrow \Gamma_7$ $^2F_{5/2}$ transition is electric-quadrupole allowed. Each transition shows rich vibrational structure, with the derived internal LnF_6^{3-} vibrational modes being at (in cm^{-1}) the following values: ν_6, 135 (zone center), 149 (zone boundary); ν_4, 169; ν_3, 376 (zone boundary), 387 (transverse optic),

* To whom correspondence should be addressed. E-mail: bhtan@cityu.edu.hk.
† City University of Hong Kong.
‡ University of Canterbury.
§ Present Address: 88 Avenue Jean Jaurès, 92140 Clamart, France.

10.1021/jp057241j CCC: $33.50
Published on Web 07/13/2006

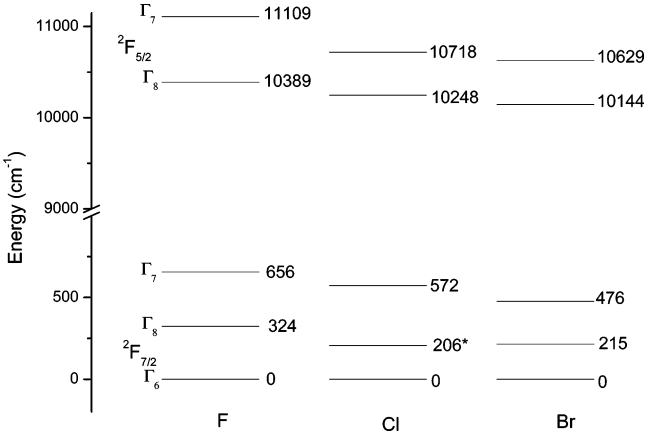

Figure 2. Energy level diagrams of the f^{13} configuration in Cs_2NaYbX_6 (X = F, Cl) and $Cs_2NaHoBr_6$:Yb^{3+}. The starred Γ_8 level for $Cs_2NaYbCl_6$ is perturbed by electron−phonon coupling with $\Gamma_6 + \nu_2$.

436 (longitudinal optic). In addition, weak lattice mode structure is observed at 53 and 66 cm^{-1} above the zero phonon lines, corresponding to the $S_9(\tau_{1u})$ and $S_5(\tau_{2g})$ unit cell group modes,[1] respectively, as well as two-phonon modes involving the 53 cm^{-1} vibration in combination with ν_6 and ν_4. This accounts for all of the 10 K-bands, except for (i) weak features at 256 ± 2 cm^{-1} above the electronic origins which correspond to the $S_8(\tau_{1u})$ vibration and (ii) very weak first members of the $S_2(\nu_2)$ vibrational progression on the electronic origin and vibronic structure, with the derived energy of 400 ± 4 cm^{-1} for ν_2.

Vibrational hot bands are observed at 60 K which are symmetric in energy with regard to the positions of the electronic origins. However at higher temperatures some new bands appear, and increase in intensity with temperature, which are due to further electronic transitions from the thermally populated crystal field levels of $^2F_{7/2}$. These bands are assigned to the $^2F_{7/2}$ $\Gamma_8 \rightarrow \Gamma_8$ $^2F_{5/2}$ zero phonon line (at 10065 cm^{-1}) and to the origin and vibronic structure of $^2F_{7/2}$ $\Gamma_7 \rightarrow \Gamma_8$ $^2F_{5/2}$. These assignments enable the complete energy level structure of the f^{13} configuration to be realized (Figure 2).

Comparison of our absorption spectrum with the room-temperature spectrum of Rb_2NaYF_6:Yb^{3+} in ref 9 enables the assignment of the $\Gamma_6 \rightarrow \Gamma_8$ transition in this system at ∼10398 cm^{-1}, which is close to the value found in this study. Our previous preparation of Cs_2KYbF_6 from anhydrous fluorides introduced some impurities into the crystals so that the zero phonon lines in the $^2F_{7/2}$ $\Gamma_6 \rightarrow \Gamma_8$, Γ_7 $^2F_{5/2}$ absorption spectra were strong and multiple, also because of the presence of defect sites.[10] However, from the vibronic analysis of this Cs_2MYbF_6 (M = K) system, the $^2F_{5/2}$ Γ_8, Γ_7 electronic states were located at 10400 and 11120 cm^{-1}, and these values are each only ∼10 cm^{-1} greater than the M = Na system herein. From the previous magnetic studies of Cs_2MYbF_6 (M = Na,K,Rb),[4] the $^2F_{5/2}$ Γ_8, Γ_7 levels were estimated at 377 and 769 cm^{-1}, and these values seem rather high.

Yb^{3+} has no single ion energy levels which can be pumped by visible or near-ultraviolet lasers. The luminescence spectrum of $Cs_2NaYbCl_6$ was achieved by excitation into the energy levels of Ho^{3+} (in $Cs_2NaHoCl_6$:Yb^{3+}) with subsequent energy transfer to the $^2F_{5/2}$ multiplet of Yb^{3+}.[8] The emission spectra of Yb^{3+} in the hosts Cs_2NaHoF_6, Cs_2NaYbF_6, and Cs_2NaYF_6 were recorded from 10 K to room temperature in the region near 1 μm using 355 or 476 nm laser excitation. Some of the 10 K spectra are shown in Figure 3. In all spectra there are multiple zero phonon lines, which correspond to defect sites, with associated vibronic structure (at ∼146, 170, 380 cm^{-1}) to lower

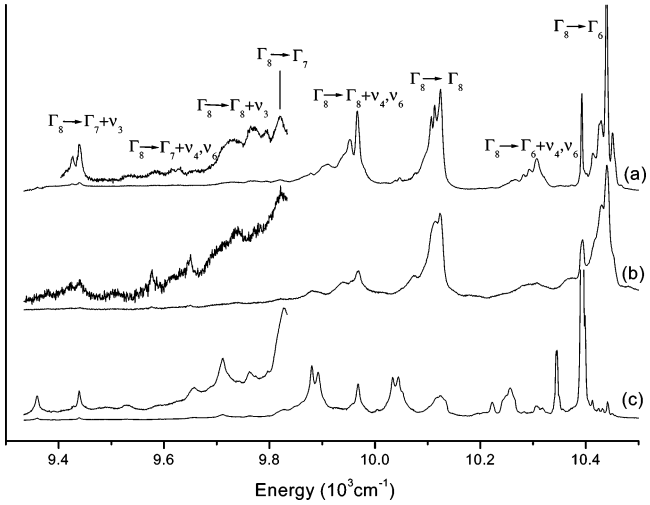

Figure 3. Emission spectra at 10 K of Yb^{3+} in elpasolite hosts: $Cs_2NaY_{0.9}Yb_{0.1}F_6$ under (a) 476 nm and (b) 355 nm excitation; (c) Cs_2NaYbF_6 excited at 477 nm. The ordinate is emission.

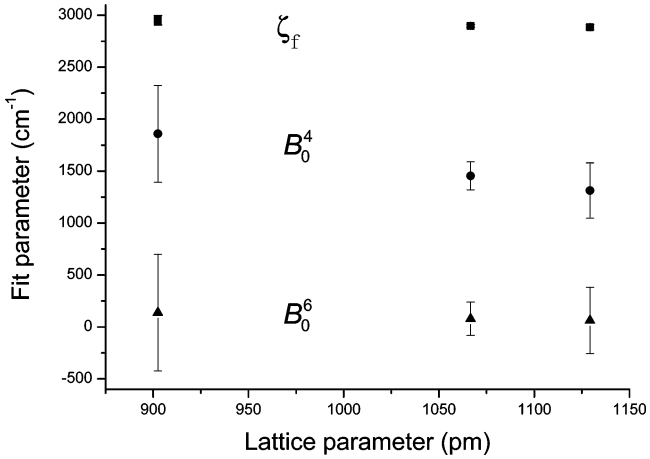

Figure 4. Spin−orbit and crystal field fitted parameters from $4f^{13}$ energy level fits plotted against the lattice parameter for YbX_6^{3-} (from left to right X = F, Cl, Br; vertical bars indicate standard deviations).

energy. The schematic assignments are depicted in Figure 3a for the 476 nm excited spectrum of Cs_2NaYF_6:Yb^{3+} (10 atom %). This excitation energy presumably corresponds to the Yb^{3+}−Yb^{3+} double ion excitation. Relative to the $\Gamma_8 \rightarrow \Gamma_6$ energies (which are between 10387 and 10467 cm^{-1}), the derived energies of the $^2F_{7/2}\Gamma_8$ and Γ_7 states are at ∼327 and 648 cm^{-1}, respectively. The bands change relative intensity with change in excitation line (Figure 3b), with increasing concentration (Figure 3c), and also with change in temperature. The emission of Cs_2NaHoF_6:Yb^{3+} is weak and also shows defect site bands so that the $Ho^{3+} \rightarrow Yb^{3+}$ energy transfer is not as favorable as in the case of $Cs_2NaHoCl_6$:Yb^{3+}.

Crystal Field Analysis of $4f^{13}$. The $4f^{13}$ system is conveniently analyzed by the parametric Hamiltonian including only the interactions of the spin−orbit (parameter: ζ_f) and the f-electron crystal field (parameters: B_0^4 and B_0^6, with $B_4^4 = \pm(5/14)^{1/2}B_0^4$ and $B_4^6 = \mp(7/2)^{1/2}B_0^6$ for the cubic symmetry site). A further parameter (E_{AVE}) may be employed to shift the whole configuration. The Reid f-shell programs were employed to fit the energy levels of YbX_6^{3-} (X = F, Cl, Br). The $^2F_{7/2}\Gamma_8$ level in $Cs_2NaYbCl_6$ is perturbed by electron phonon coupling, and a simple correction has been made for this.[11] The calculated energy levels are listed in Table 1, and the derived parameters are given in Table 2. Although the trends in parameter values are reasonable (Figure 4), the standard deviations of the fittings

TABLE 1: Energy Levels (cm^{-1}) of Yb^{3+} in Elpasolite Lattices[a]

			Cs_2NaYbF_6		$Cs_2NaYbCl_6$		$Cs_2NaYbBr_6$	
Cf	$^{2S+1}L_J$	IR	exptl	calcd	exptl	calcd	exptl	calcd
$4f^{13}np^6$	$^2F_{7/2}$	Γ_6	0	−48	0	−14	0	−29
		Γ_8	324	294	250	242	215	200
		Γ_7	656	734	572	594	476	520
	$^2F_{5/2}$	Γ_8	10389	10484	10248	10276	10144	10199
		Γ_7	11109	11014	10718	10690	10629	10574
$4f^{14}np^5$	$^2P_{3/2}$	Γ_8	50000		35850		28000	
	$^2P_{1/2}$	Γ_6	(50535)		(37201)		(33024)	
				s.d. = 166		s.d. = 48		s.d. = 95

[a] Configuration (Cf), irreducible representation (IR), experimental (exptl) energy, and calculated (calcd) energy in $4f^{13}np^6$ using the parameters in Table 2. The $^2F_{5/2}\Gamma_8$ level in $Cs_2NaYbCl_6$ has been corrected for electron−phonon coupling; s.d. is standard deviation of energy level fit with five parameters. Columns 4, 6, and 8 list the experimental energies which are equal to those calculated in $4f^{13}np^6 + 4f^{14}np^5$. The calculated energy of $^2P_{1/2}$ in $4f^{13}np^6 + 4f^{14}np^5$ is shown in parentheses.

TABLE 2: Energy Parameter Values for Yb^{3+} in Elpasolite Lattices[a]

	value (cm^{-1})									
	Cs_2NaYbF_6		$Cs_2NaYbCl_6$		$Cs_2NaYbBr_6$		$Cs_2NaTmCl_6$		$Cs_2NaErCl_6$	
parameter	$4f^{13}np^6$	$4f^{14}np^5$	$4f^{13}np^6$	$4f^{14}np^5$	$4f^{13}np^6$	$4f^{14}np^5$	$4f^{13}np^6$	$4f^{14}np^5$	$4f^{13}np^6$	$4f^{14}np^5$
E_{AVE}	4751	5516	4615	4763	4552	4734				
ζ_f	2952	2995	2898	2910	2885	2908	2616	2634	2363	2394
$B_0^4(f,f)$	1859	−2083	1454	699	1313	412	1787	795	1555	944
$B_0^6(f,f)$	138	−859	79	−90	63	−53	170	−25	154	55
ΔE_{AVE}		42856		31186		24501		31500		29268
ζ_p	-	[560]	-	[960]	-	[3478]	-	[1000]	-	4154
$B_0^4(f,p)$	-	±30438	-	±11287	-	±10925	-	−11514	-	−10244

[a] Constrained values are shown between square brackets.

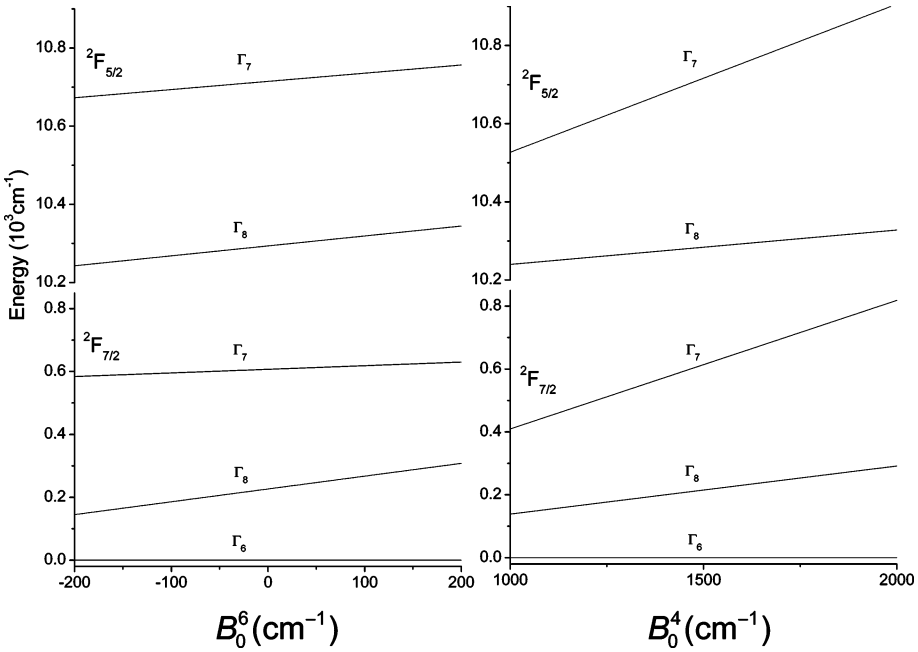

Figure 5. Change in calculated energies of $Cs_2NaYbCl_6$ as a function of $B_0^6$and B_0^4 for $4f^{13}$ energy level fits. The value of ζ_f is 2903 cm^{-1}. The value of $B_0^4(f,f)$ is 1473 cm^{-1} when $B_0^6(f,f)$ is varied, and the value of $B_0^6(f,f)$ is −39 cm^{-1} when $B_0^4(f,f)$ is varied.

(Table 1) and of the parameter values (Table 2) are large. This is surprising because 5 energy levels are being fitted by 4 parameters. Figure 5 shows that the splitting of $^2F_{5/2}$ is independent of the value of B_0^6, and whereas the energy separation of the levels $^2F_{7/2}$ Γ_7, Γ_8 decreases with increasing B_0^6, it increases with increasing B_0^4.

Inclusion of Configuration Interaction in the Crystal Field Analysis. Following the same approach as in ref 12 and 13, we have assumed that an interaction taking place between the nearly filled 4f orbital and the molecular orbitals localized on the halide ligands is responsible for the mediocre agreement between the $4f^{13}$ crystal field calculation and the experimental levels. This interaction can be simulated by evaluating the perturbation caused by the $4f^{14}np^5$ configuration on $4f^{13}np^6$ (where $n = 2$, 3, 4 for F, Cl, Br, respectively). The result will be numerically the same if the perturbation is calculated between the mirror configurations $4f^1np^0$ and $4f^0np^1$ provided the signs of one-particle parameters are reversed. The matrix to be solved contains the 14 4f states ($^2F_{7/2}$ and $^2F_{5/2}$) and the six np states ($^2P_{3/2}$ and $^2P_{1/2}$). The relevant interactions are the central field,

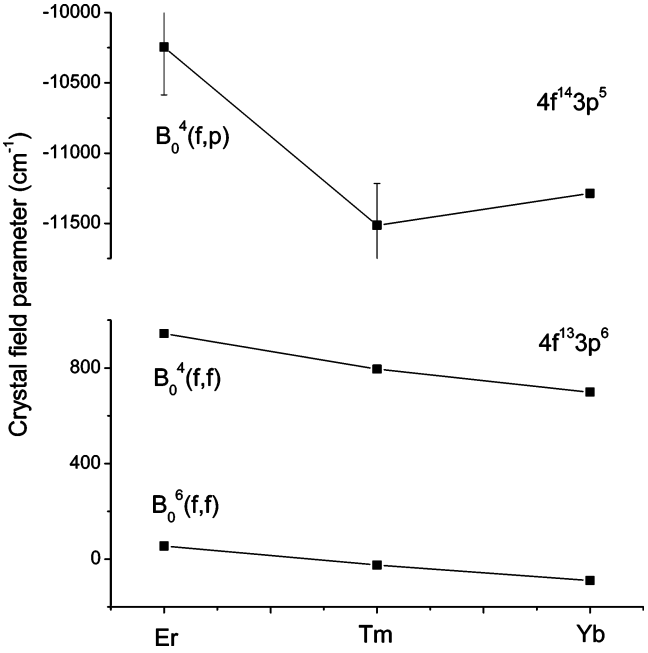

Figure 6. Variation of B_0^4(f,f), B_0^6(f,f), and B_0^4(f,p) in $Cs_2NaLnCl_6$ for Ln = Er, Tm, Yb from the energy fits including configuration interaction.

the spin−orbit, and the crystal field interactions. The parameters involved are E_{AVE}, ζ_f, B_0^4(f,f), B_0^6(f,f), and in addition ζ_p, B_0^4(fp) and the gap ΔE_{AVE} between the two configurations. Ryan and Jørgensen[14] pointed out that the charge-transfer spectra of YbX_6^{3-} are due to electron transfer from the highest filled molecular orbital mainly localized on the halide ligands to the partly filled 4f orbitals. The offset of the charge transfer band, when experimentally available, determines the energy gap. It is close to 28 000 and 35 850 cm^{-1} for $YbBr_6^{3-}$ and $YbCl_6^{3-}$, respectively. The band was not reported for YbF_6^{3-} but is larger than 50 000 cm^{-1}.[14] The parameter ζ_p is ascribed the value of the spin−orbit coupling constant of a p electron in $2p^6$ (Ne), $3p^6$ (Ar), and $4p^6$ (Kr), that is, 560, 960, and 3478 cm^{-1}, respectively. We are left with five parameters E_{AVE}, ζ_f, B_0^4(f,f), B_0^6(f,f), and B_0^4(f,p) to fit the five 4f levels. The interaction with $4f^{14}np^5$ expands the upper $^2F_{5/2}$ multiplet with respect to $^2F_{7/2}$.On including the configuration interaction, and fitting with five parameters, of course the calculated energy levels match exactly the experimental levels listed in Table 1. The calculated energy of the $^2P_{1/2}$ level of the $4f^{14}np^5$ configuration is listed in Table 1 between parentheses. The corresponding energy parameters are given in Table 2 and compared with those for $Cs_2NaErCl_6$[12] and $Cs_2NaTmCl_6$.[13] The parameters in column 9 differ from those listed in Table 3 of ref 13 for the following reason. The parameters listed in the latter table were such that the mean deviation was a minimum (9.3 cm^{-1}). The ΔE_{AVE} was therefore set equal to 38 500 cm^{-1}, and the calculated energy level scheme displayed a gap in the 38000−54000 cm^{-1} region. However it was pointed out that a small hump is present at 47600−50000 cm^{-1} in the ultraviolet absorption spectrum, which we assign to the offset of the $4f^{14}3p^5$ configuration.[14] Thus, the calculation agrees with this hypothesis if ΔE_{AVE} is lowered down to 31 500 cm^{-1}. The mean deviation only increases slightly to 10.6 cm^{-1}, and the offset of the excited configuration occurs between 46 840 and 58 529 cm^{-1}, which is consistent with experiment. The fitted parameters for $Cs_2NaTmCl_6$ are listed in column 9 of Table 2.

Figure 6 shows the variation of B_0^4(f,f), B_0^6(f,f), and B_0^4(f,p) in $Cs_2NaLnCl_6$ for Ln = Er, Tm, Yb from the energy fits including configuration interaction. The smooth variation supports the assumption which has been made concerning the refinement of the energy level calculation by including configuration interaction. It shows that the experimental determination of the charge-transfer band is essential to augment the accuracy of the calculation method. Actually, the absorption bands are due to the transitions to gerade states of the charge-transfer configuration, whereas the configuration interaction with $4f^{13}$ involves ungerade states.

Conclusions

The well-resolved electronic absorption spectrum of octahedrally coordinated Yb^{3+} in Cs_2NaYbF_6 has enabled the $4f^{13}$ energy level diagram to be deduced. By contrast, the emission spectra recorded under ultraviolet and visible laser excitation show multiple structures associated with various defect sites. The comparison of the derived energy levels from the present study with those from YbX_6^{3-} (X = Cl, Br)[11] is made in Figure 2. Although the energy level fitting is not precise, the expected trends in derived parameter values are manifested across the series YbX_6^{3-} (X = F, Cl, Br). Inclusion of configuration interaction with the charge-transfer configuration gives an exact energy level datafit and indicates consistent trends in parameter values for the $Cs_2NaLnCl_6$ (Ln = Er, Tm, Yb) systems.

Acknowledgment. Financial support of this work under City University Research Grant 9360099 is gratefully acknowledged.

References and Notes

(1) Tanner, P. A. *Top. Curr. Chem.* **2004**, *241*, 167.
(2) Becker, R.; Lentz, A.; Sawodny, W. *Z. Anorg. Allg. Chem.* **1976**, *420*, 210.
(3) Bucher, E.; Guggenheim, H. J.; Andres, K.; Hull, G. W.; Cooper, A. S. *Phys. Rev. B: Condens. Matter Mater. Phys.* **1974**, *10*, 2945.
(4) Urland, W. *Z. Naturforsch., A: Phys. Sci.* **1979**, *34*, 1507.
(5) Tanner, P. A.; Liu, Y.-L.; Edelstein, N.; Murdoch, K.; Khaidukov, N. M. *J. Phys.: Condens. Matter* **1997**, *9*, 7817.
(6) Thorne, J. R. G.; Jones, M.; McCaw, C. S.; Murdoch, K. M.; Denning, R. G.; Khaidukov, N. M. *J. Phys.: Condens. Matter*. **1999**, *11*, 7851.
(7) Berry, A. J.; Morrison, I. D.; Denning, R. G. *Mol. Phys.* **1998**, *93*, 1.
(8) Tanner, P. A. *Mol. Phys.* **1986**, *58*, 317.
(9) DeLoach, L. D.; Payne, S. A.; Chase, L. L.; Smith, L. K.; Kway, W. L.; Krupke, W. F. *IEEE J. Quantum Electron.* **1993**, *29*, 1179.
(10) Acevedo, R.; Tanner, P. A.; Meruane, T.; Poblete, V. *Phys. Rev. B: Condens. Matter Mater. Phys.* **1996**, *54*, 3976.
(11) Tanner, P. A.; Kumar, V. V. R. K.; Jayasankar, C. K.; Reid, M. F. *J. Alloys Compds.* **1994**, *215*, 349.
(12) Faucher, M. D.; Tanner, P. A. *Mol. Phys.* **2003**, *101*, 983.
(13) Faucher, M. D.; Tanner, P. A.; Mak, C. S. K. *J. Phys. Chem. A* **2004**, *108*, 5278.
(14) Ryan, J. L.; Jørgensen, C. K. *J. Phys. Chem.* **1966**, *70*, 2845.